Non-isothermal crystallization kinetics and its effect on the mechanical properties of homopolymer isotactic polypropylene

S. Nouira[1,2] · T. Hassine[2] · J. Fitoussi[1] · M. Shirinbayan[1] · F. Gamaoun[3] · A. Tcharkhtchi[1]

Abstract
The non-isothermal crystallization of the isotactic Polypropylene (iPP) was studied using differential scanning calorimetry and polarizing optical microscopy. Jeziorny's model and Ozawa's theoretical approaches were applied to study the non-isothermal kinetics of the iPP. Jeziorny's approach proved to be the most relevant model to the present material. Simultaneously, the activation energy was calculated with Kissinger's method and Vyazovkin's iso-conversional approach. Indeed, the latter provides an activation energy varying between 100 and 176 kJ/mol. Furthermore, the WAXD scans indicated the presence of a single crystalline form in the used material. To study the effect of the microstructure on the mechanical properties of the iPP, multiscale tensile tests were carried out for different film microstructures. At macroscopic scale, the increase in the diameter of spherulites, inevitably accompanied by a rise in the crystallinity rate, induces the growth of rigidity, brittleness, and elastic limit. Moreover, the results of the in-situ micro-tensile tests present the evolution of spherulites during loading.

Keywords Polypropylene · Crystallization · Mechanical characteristics

Introduction

Over the past years, plastic implementation has been used in multiple applications. The replacement of metal parts with polymeric ones in new technological devices and machines has become increasingly significant [1]. Many researchers have found thermoplastics attractive thanks to their mechanical and physical properties as well as their potential to be recycled. In particular, polypropylene with different tacticity has been used due to the high variability in their stereo-regularity. We can find syndiotactic, atactic and isotactic polypropylene.

The most commercial one is the isotactic Polypropylene (iPP), thanks to its good regularity and high tendency towards crystallization. Its usage has to expand in the automotive and mechanical fields [2]. It is a semicrystalline polymer, it has a relatively low density and a low price, excellent moisture, ease of processability, high toughness and chemical resistance [3]. Its favorable mechanical and physico-chemical properties contribute to its high rate of use and enhance the control of its properties by varying the processing parameters [4].

In the iPP, the pendent groups are on the same side of the carbon, which results in helicoidal determination,

✉ S. Nouira
samia.nouira@ensam.eu

T. Hassine
tarek.hassine@eniso.u-sousse.tn

J. Fitoussi
joseph.fitoussi@ensam.eu

M. Shirinbayan
mohammadali.shirinbayan@ensam.eu

F. Gamaoun
fgamaoun@kku.edu.sa

A. Tcharkhtchi
abbas.tcharkhtchi@ensam.eu

[1] Arts Et Metiers Institute of Technology, CNAM, PIMM, HESAM University, 75013 Paris, France

[2] National Engineering School of Sousse ENISO, Mechanical Laboratory of Sousse LMS, University of Sousse, Sousse, Tunisia

[3] Department of Mechanical Engineering, College of Engineering, King Khalid University, Abha 61421, Saudi Arabia

folded to form thin and ordered structures. Depending on the mechanical and thermal conditions, the material states range from practical amorphism when melted to high crystallinity (ordered structure with different crystalline forms). We can find four forms in an iPP: monoclinic (α), hexagonal (β), triclinic (γ), and mesophase. The latter has been reported under critical conditions [5]. It is well known that parameters like the cooling rate influence the microstructure of semi-crystalline polymers, so that the control of crystallization during the solidification process of a thermoplastic material is of major importance to achieve optimal properties of a cured polymer [6, 7].

In general, crystallization studies have been limited to idealized conditions, hence neglecting in the external factors like the cooling rate and the thermal gradient [8]; but in real situations, industrial processes take place in continuously changing conditions, thus making the study of a polymer microstructure more complex [9, 10].

In fact, in order to properly describe the usual processing conditions and the solidification phase during manufacturing, efforts have been focused on understanding the non-isothermal crystallization – by changing the cooling rates – to describe the behavior of semicrystalline polymers for various temperatures [11, 12]. Consequently, it is important to study the kinetics and melting behavior after solidification to generate microstructural knowledge that can be investigated to operate industrial manufacturing processes to have final products with improved properties.

Most global crystallization models, whether under isothermal or non-isothermal conditions, have been based on work carried out between 1930 and 1940s by Kolmogorov, Avrami and Evans. These models have determined the relative transformation rate (X) which corresponds to the fraction of a considered volume, which will be transformed into a crystalline volume as a function of time or temperature. Avrami's model has been used universally to describe polymer crystallization kinetics due to its simple application. In many cases, isothermal models are experimentally available only on a narrow temperature range, which does not correspond to industrial conditions [13]. Therefore, non-isothermal modeling is primordial to understand the behavior crystallization of semi-crystalline polymers. Different modifications of Avrami's equation have been made to study the non-isothermal crystallization kinetics of semi-crystalline polymers. We can use Jeziorny's model, Nakamura's model, Ozawa's model and Mo's model to describe this phenomenon [14].

A lot of studies have investigated the crystallization kinetics of the iPP. Mubarak et al. [15] investigated the non-isothermal crystallization studies of the iPP by comparing Nakamura's model and Ozawa's model. They suggested that for a wide range of cooling rates Nakamura's model is not successful in describing the non-isothermal crystallization kinetics of the iPP and they concluded that Ozawa's model could best describe it. Layachi et al. [16] studied also the non-isothermal crystallization kinetics of the iPP by comparing Avrami's model modified by Jeziorny, Ozawa's model and Mo's model. They suggested that Jeziorny and Ozawa's approaches could clearly describe the kinetics of the iPP.

As mentioned before, the mechanical properties of thermoplastic polymers significantly depend on the microstructure parameters, such as the type of spherulites and the degree of crystallinity. Like any transformation phase, crystallization abides by the laws of thermodynamics [17, 18]. The size of crystals depends on the control of thermal heat processing. Several researchers confirmed that a slow-cooled rate released for a fully developed crystalline structure would reveal better mechanical properties [19–23]. In order to better predict the mechanical properties of semi-crystalline thermoplastics, it seems important to quantify and understand the effect of structural parameters such as the degree of crystallinity and the crystal size on the mechanical properties [24], including resilience, toughness and Young's modulus. Mahmood et al. [25] and Dietz [26] studied the effect of the internal structure of an injection-molded sample on the mechanical properties of the iPP. They showed an interrelation between the degree of crystallinity and the local cooling rates, and so the effect on the toughness and storage modulus of the polymer. In order to better analyze the microstructure under tensile tests, the tensile deformation mechanisms of the polypropylene were imaged by an optical microscope with an original micro-tensile machine.

In this work, the non-isothermal crystallization kinetics of the iPP have been studied. Then, different methodologies were employed to evaluate the non-isothermal crystallization behavior, such as Differential Scanning Calorimetry (DSC) and polarized optical microscopy. Specific theoretical approaches were also employed to model the non-isothermal kinetics of the iPP. Generally, the obtained results of various methods are controversial, especially when theoretical approximations and experimental conditions are not clear. Finally, the mechanical characteristics such as resilience and Young's modulus were analyzed for polymer films with different microstructures.

Experimental procedure

Materials

In the present study, a commercial iPP homopolymer, provided by Chemieuro with the commercial name PPH 4060, was used. It exhibited a flow index of 3 g 10 min^{-1} and a melting density of 0.905 gr cm^{-3}. The percentage of isotacticity of the used polymer was estimated at 98% utilizing a Perkin Elmer FTIR Frontier spectrometer from 4000 to

400 cm^{-3} in ATR (Attenuated Total Reflectance), equipped with a diamond/ ZnSe crystal.

Preparation of polypropylene films

For crystallization studies, polymer films with different thicknesses were prepared. A process of molding and heating in a thermocompression was performed. For each desired thickness, a wedge was placed between two sheets of Kapton. After that, a pressure of 200 bars was applied at a temperature of 210 °C for 5 min.

Differential scanning calorimetry

Calorimetric data of non-isothermal crystallization were obtained using a DSC machine (Q1000 V9.0 Build 275 TA instruments). Before testing, indium was used to calibrate the temperature scale and the melting enthalpies. Nitrogen gas was purged into the DSC cell with a constant flow rate of 50 ml min^{-1}, to avoid material oxidation. The sample weight was 6 ± 0.5 mg using a balance Mettler Toledo with 0.01 mg sensitivity.

Specimens were crimped in non-hermetic aluminum pans, while sealed and heated at a rate of 20 °C min^{-1} to 210 °C for 3 min. This procedure was used to delete the thermal history of the polymer. For non-isothermal crystallization studies, previously heated samples were cooled down at various cool

Evaluation of tensile properties

Macroscopic tensile tests

The mechanical characteristics such as resilience and Young's modulus were analyzed for different microstructures of the semi-crystalline polymer. The tensile properties were measured with 1BB specimens using Instron 5966 with loading capacity of 10 KN and a loading rate of 10 mm min^{-1}.

In-situ tensile tests

The machine of micro-traction, presented in Fig. 1, was used to follow the evolution of the morphology at the same zone during the tensile deformation by pulling from two sides to establish a chronology of the deformation mechanisms. The images were captured during testing at every second to present the change in the microstructure.

Experimental results and discussions

Non-isothermal crystallization analysis

From non-isothermal crystallization experiments, and at each cooling rate, dynamic DSC data for the crystallization exotherms as a function of temperature can be obtained, as reported in Fig. 2.

As expected, when the cooling rate increases, the crystallization exotherm becomes broader and the peak of crystallization temperature, $T_{0,}$ shifts progressively to lower temperatures. Some characteristic parameters are represented in Table 1 for each cooling rate ϕ. As expected, all the characteristic temperature values decrease with the rising cooling rate: The starting crystallization process will be completed first.

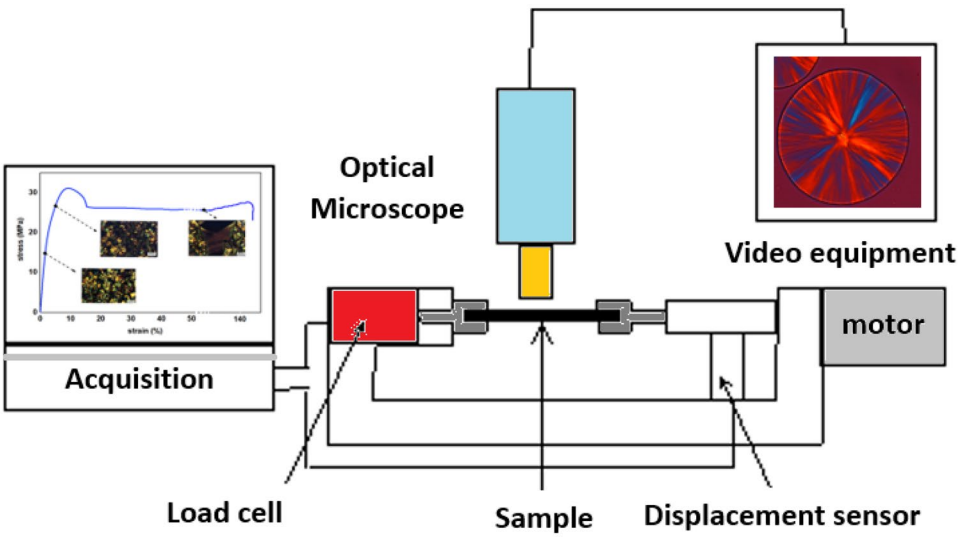

Fig. 1 Procedure of in-situ tensile tests

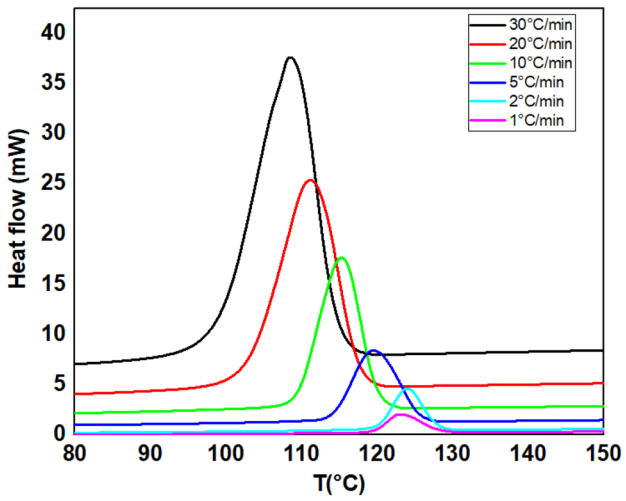

Fig. 2 Non-isothermal crystallization exotherms of neat iPP

Based on the assumption that the evolution of crystallinity is linearly proportional to the evolution of heat release during crystallization, the transformation ratio of the material from the melting state to the crystal one, namely relative crystallinity, can be determined using DSC data [27] as a function of time or temperature for the different cooling rates and according to the following expression:

$$X(t) = \frac{\int_{T_{onset}}^{T} \frac{\Delta H_{c(t)}}{dt} dt}{\int_{T_{onset}}^{T_{\infty}} \frac{\Delta H_{c(tot)}}{dt} dt} \quad (1)$$

where T_{onset} denotes the beginning of the crystallization phenomena, T_{∞} holds for the final temperature of the crystallization exotherm, ΔH_c represents the enthalpy of the crystallization released with an infinitesimal dT temperature, T represents the crystallization temperature at time t, T_{onset} and T∞ correspond to the overall enthalpy of crystallization during the transformation phase. Relative crystallinity can be represented as a function of time using the following relation:

$$t = \frac{Tonset - T}{\phi} \quad (2)$$

Table 1 T_0 crystallization temperature, and T_{onset} and T_{∞} temperatures.of neat iPP at various ϕ cooling rates

Cooling rates (°C min^{-1})	T_c (°C)	T_{onset}(°C)	T_{∞}
30	108.47	115.10	88
20	111.1	117.85	97
10	115.28	120.33	107
5	119.5	125.76	111

where ϕ is the cooling rate. This relationship is valid when the sample probably has the same thermal history as the DSC furnace [28].

Figure 3 represents the variation in the relative degree of crystallinity of the iPP, where X(T) can be converted to X(t) using Eq. (2) at different cooling rates. The obtained curves reveal a similar sigmoidal shape: the three regimes during crystallization phenomena [17, 29, 30]. The beginning of the transformation at a low slope for high-temperature values corresponds to the nucleation and the formation of a sufficient number of crystallites. During this period, the relative crystallinity does not change. The second stage corresponds to the phase of the growth of spherulites. The rate of their growth is directly related to the rate of cooling. This period is more important for the greatest cooling rate. The third step corresponds to the final phase of the process [31]. During this stage, the spherulites interact with each other to form solid polygons at the end of crystallization.

The quantity of non-transformed material is reduced, and the appearance of new nuclei drops, hence the growth of spherulites. We can see that the overall crystallization temperature range decreases with the increase in the cooling rate.

Jeziorny's analysis of non-isothermal crystallization

To quantitatively describe the evolution of crystallinity and polymer behavior during non-isothermal crystallization, we can apply different kinetic models, for instance Avrami's, Ozawa's and Mo's. Avrami's microkinetic approach is one of the most used theories in the field and can be employed to analyze the isothermal crystallization behavior of the polymer based on the following equation:

$$1 - X(t) = \exp(-Zt^n) \quad (3)$$

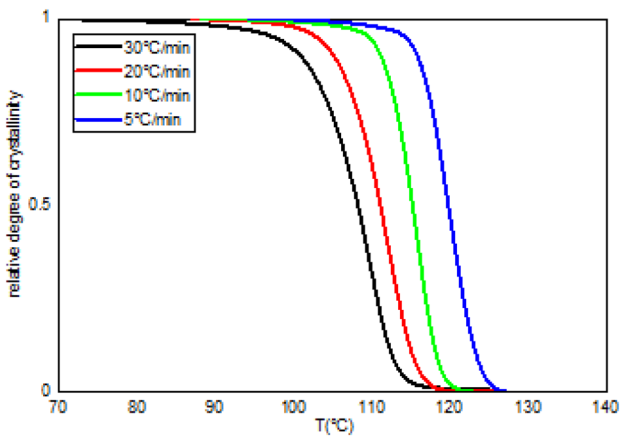

Fig. 3 Avrami's plots: Evolution of relative crystallinity as a function temperature

where X(t) represents the degree of relative crystallinity at time t, Z is the crystallization rate constant depending on growth rate, and n is Avrami's crystallization exponent representing the morphology of crystals and the nature of nucleation (homogeneous or heterogenous nucleation) [32–34]. Parameters Z and n are estimated by taking the logarithmic of Eq. (3) so as to have a linear fitting transformation, as shown in Eq. (4):

$$\ln\left(-\ln\left(1-X(t)\right)\right) = \ln(Z) + n\ln(t) \tag{4}$$

Therefore, $\ln\left(-\ln\left(1-X(t)\right)\right)$ plotted versus $\ln(t)$ yields Avrami's parameters n and Z via the slope and intercept of the linear plots, respectively. To account for the non-isothermal crystallization conditions, Avrami's approach was modified by Jeziorny, introducing the cooling rate ϕ as $\ln Z_J = \frac{\ln Z}{\phi}$ [35, 36].

To avoid the secondary crystallization and the impingement of spherulites; Jeziorny-Avrami's modified approach was used for X(t) ϵ [0.1;0.8]. Avrami's analysis results are presented in Fig. 4. A high correlation ($R^2 > 0.99$) can be seen indicating the efficiency of Avrami's approach modified by Jeziorny for the description of the non-isothermal crystallization kinetics of the polymer. Table 2 summarizes the main kinetic parameters deduced from Avrami and Jeziorny's analysis.

The n values are in the vicinity of 2.2–2.5, similar to most literature reports [37–39], and they are interpreted as two-dimensional spherulitic growth with heterogeneous nucleation. Moreover, the increase in Avami's exponent while decreasing the cooling rate is indicative of the sporadic nucleation phenomenon. However, Z_J, which is the crystallization rate, goes up with the rising cooling rate, indicating the increase in the transformation rate.

Table 2 Non-isothermal crystallization kinetics parameters for iPP using DSC results

Cooling rate (°C min^{-1})	Z_J	n	R^2
30	1.1	2.24	0.999
20	1.09	2.25	0.999
10	1.08	2.37	0.999
5	0.84	2.38	0.998

Alternatives to Avrami's approach for non-isothermal crystallization

The non-isothermal crystallization results were also compared with Ozawa's approach [40]. In fact, it is a modification of Avrami's theory which directly considers the cooling rate of crystallization. The approach mentions that a non-isothermal process is a succession of infinitesimal steps of isothermal crystallization. Ozawa's equation can be obtained by applying a derivation of Evans' approach [41] to Avrami's equation:

$$1 - X(T) = exp(-R(T)/\phi m) \tag{5}$$

where R(T) denotes the cooling rate function that depends on the temperature during the thermal analysis, and m represents Ozawa's exponent.

At a fixed temperature and for different cooling rates, Ozawa's parameters are determined from the plot of ln(-ln(1-X(T)) versus ln(ϕ), as reported in Fig. 5. The limit of Ozawa's method is that the linearity regression is observed for a very restricted range of cooling rates. Hence, the analysis using Ozawa's model depends on the variation between

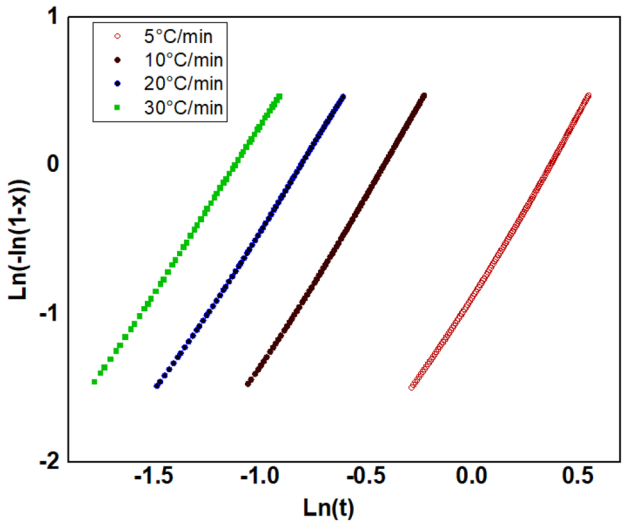

Fig. 4 Jeziorny's approach for iPP

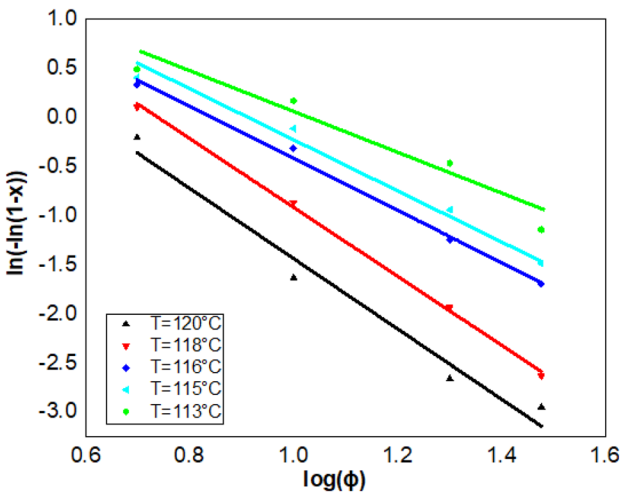

Fig. 5 Plots of ln(-ln(1-X)) versus log(ϕ) for iPP at different crystallization temperatures

Table 3 Ozawa's parameters fitted for non-isothermal crystallization kinetics of iPP

T/°C	Log (***R***(***T***))	m	R^2
113	2.08	2.04	0.9398
115	2.19	2.44	0.9850
116	2.23	2.64	0.9942
118	2.58	3.50	0.9975
120	2.13	3.57	0.9738

the primary and secondary crystallization processes. Most of the high crystallization temperatures vary linearly over a wide range of cooling rates as it is difficult for the polymer to enter the secondary crystallization phase. Table 3 summarizes the different Ozawa's parameters, by which the evolution of Ozawa's exponent m, obtained from the slopes of the different straight segments, does not show a clear tendency, thus a morphological interpretation would-be uncertain [42].

Activation energy: Kissinger's approach and iso-conversional method

The activation energy represents the minimal amount of energy required to activate the molecules of the material to accomplish a chemical transformation. Kissinger's approach [43] estimates the activation energy at several non-isothermal steps at a constant cooling rate, presented as follows:

$$\frac{d\left[\ln\left(\frac{\phi}{T_P^2}\right)\right]}{d\left(\frac{1}{T_P}\right)} = -\frac{\Delta E}{R} \tag{6}$$

where ϕ is the crystallization rate, T_p is the peak of the exotherm of DSC data, ΔE presents the activation energy of the non-isothermal crystallization, and R = 8.31 J K^{-1} mol^{-1} is the gas constant.

According to this equation, a plot of $\ln\left(\phi/T_P^2\right)$ versus $1/T_P$ should lead to a straight line with -ΔE/R as a slope. The value of the activation energy of the iPP in non-isothermal crystallization is 200 J K^{-1} mol^{-1}. The sign of energy shows the increase in the crystallization rates with the decrease in the crystallization temperature. Kissinger's approach is widely used to determine the activation energy of polymers, but it can counter several problems, as it considers the macroscopic crystallization rate, ϕ, which includes the nucleation rate and the nucleation growth, hence having different activation energy. The use of multiple cooling rates, such as the iso-conversional method, is recommended. This method can be applied to non-isothermal crystallization to evaluate the dependence of the effective activation energy on the temperature and the conversion. The iso-conversional methods, frequently used to determine the effective energy, are the differential iso-conversional methods of Friedman and the advanced Iso-conversional method of Vyazovkin et al. In this study, effective activation energy was calculated using Vyazovkin and Sbirrazzuoli approach [44, 45]. Indeed, the latter considers that the energy barrier of crystallization can vary during the non-isothermal crystallization from melting [12] using Eq. (7).

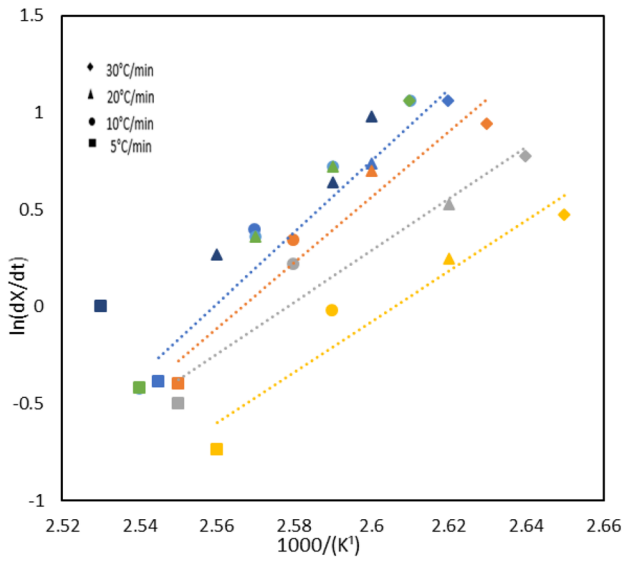

Fig. 6 Plots of ln(dX/dt) versus 1/T at constant cooling rates and different degrees of crystallinity (yellow, grey, orange, blue and green correspond to 0.8, 0.7, 0.6, 0.5 and 0.4 values, respectively)

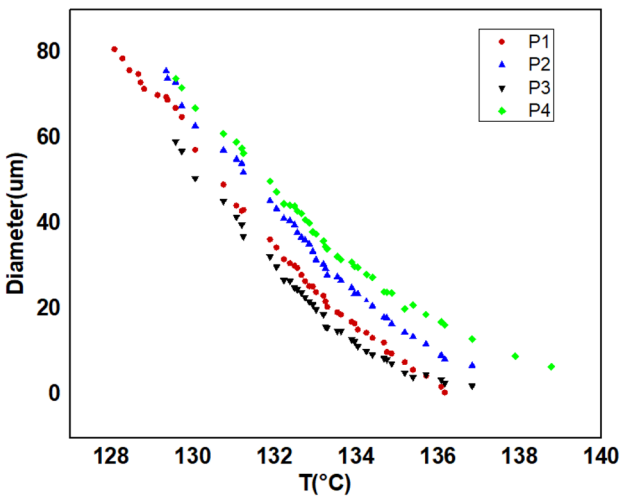

Fig. 7 Evolution of diameter of different spherulites in the same film with 150 µm thickness

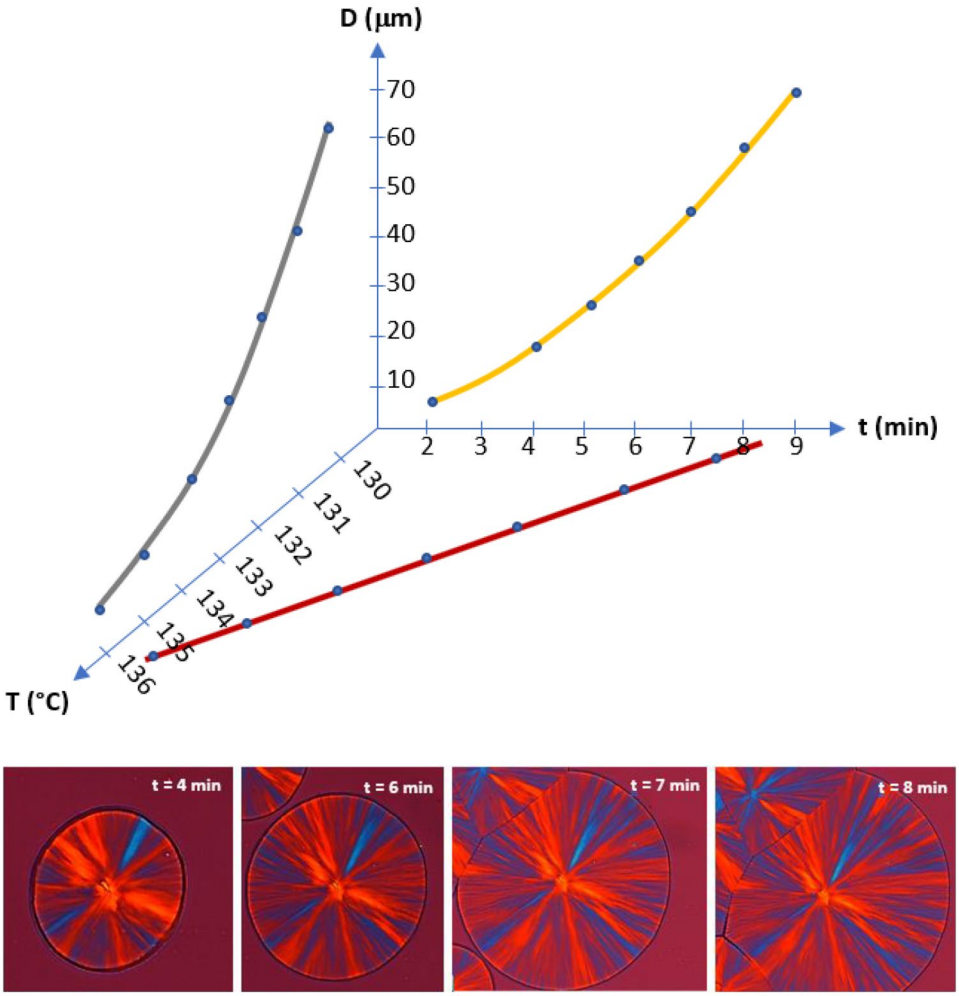

Fig. 8 Time–temperature-diameter diagram of spherulite in a sample with 100-µm thickness

$$\ln\left(\frac{dX}{dt}\right)_{X,i} = A - \frac{\Delta E_X}{RT_{X,i}} \tag{7}$$

where $\frac{dX}{dt}$ is the instantaneous crystallization rate, as a function of time at a given degree of relative X crystallinity, and ΔE_X is the activation energy related to a given conversion at different cooling rates and for a narrow temperature range.

According to this relation, the slopes deduced from the obtained linear plots of $ln(dX/dt)$ versus 1/T (Fig. 6) give ΔE_X. The deduced values of the activation energy vary between -100 kJ mol^{-1} and -176.35 kJ mol^{-1}, which covers a wide range of activation energy. Other studies concerning the iPP have revealed a similar variation with a range from -61.3 kJ mol^{-1} to -210 kJ mol^{-1} [46, 47]. The isoconversional methods take into account the variation in the activation energy with crystallization phases.

Microscopic analysis of non-isothermal crystallization

The non-isothermal crystallization analysis of the polymer (from the melting point) must be performed carefully in order to adequately control the sample temperature. Thermal gradients in between the cooling furnace and the polymer can result in an inaccurate control of the material temperature. In addition,

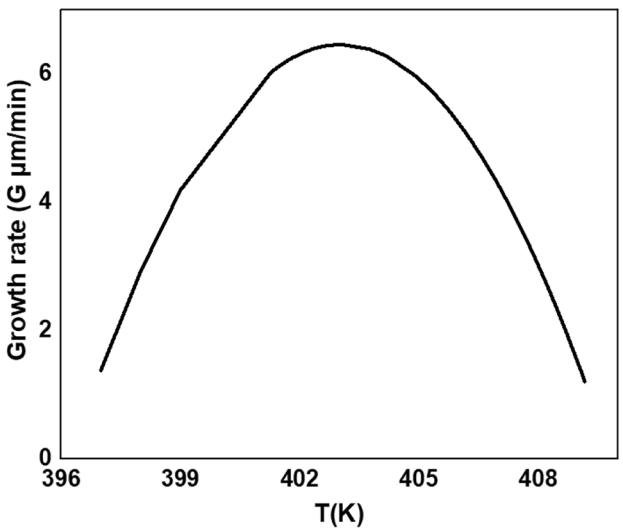

Fig. 9 Growth rate of iPP using polarizing optical microscopy

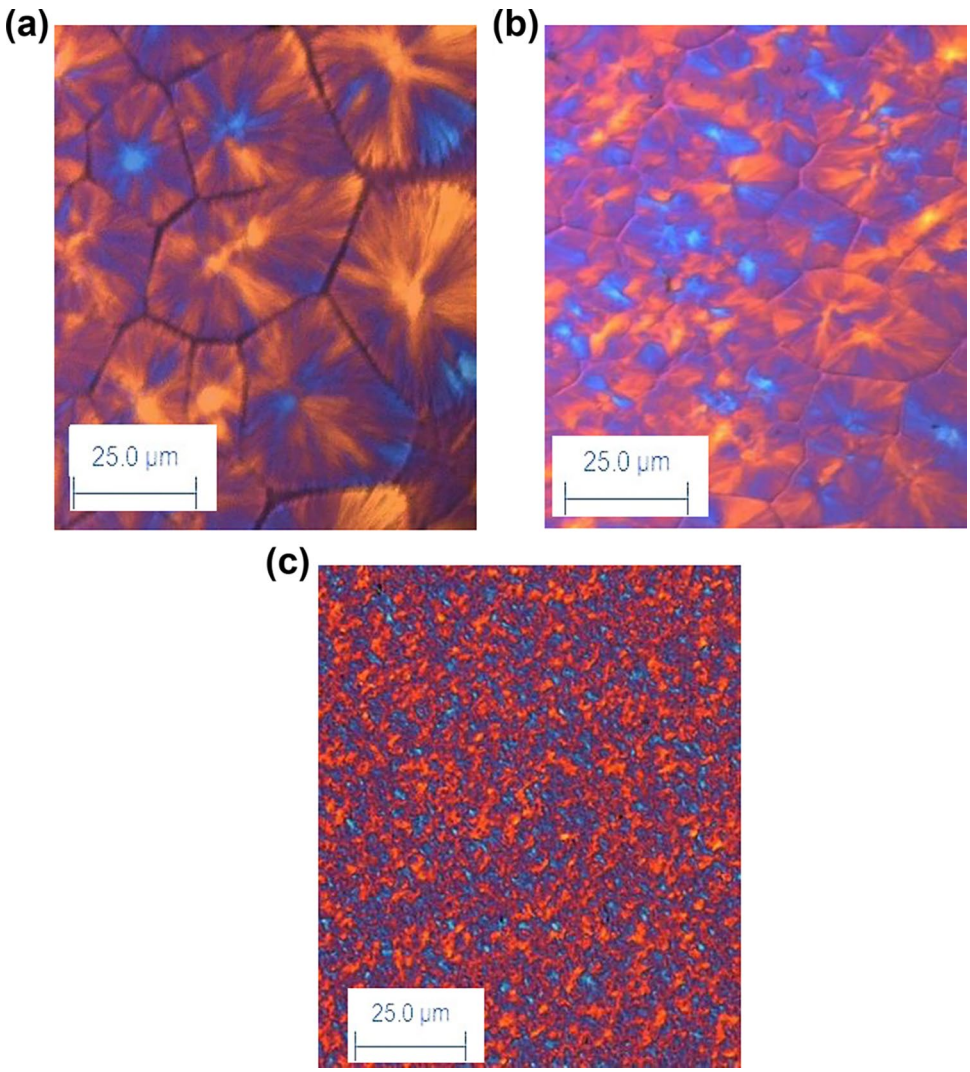

Fig. 10 Optical micrographs taken at the end of exothermal peaks of iPP performed at cooling rates of 1 °C min^{-1} (a), 5 °C min^{-1} (b) and 30 °C min^{-1} (c)

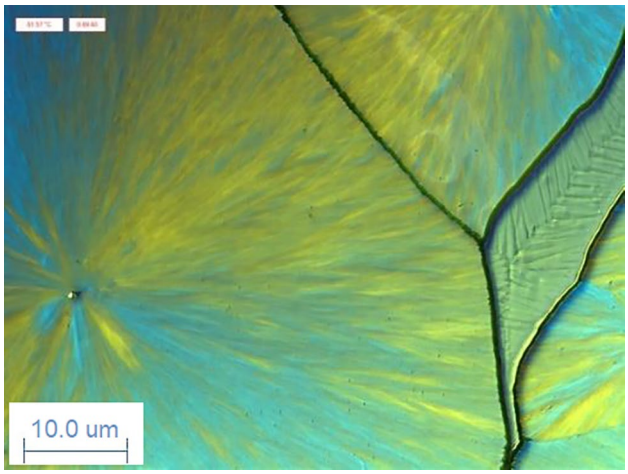

Fig. 11 Results of exothermal peaks at cooling rate of 0.5 °C min^{-1}

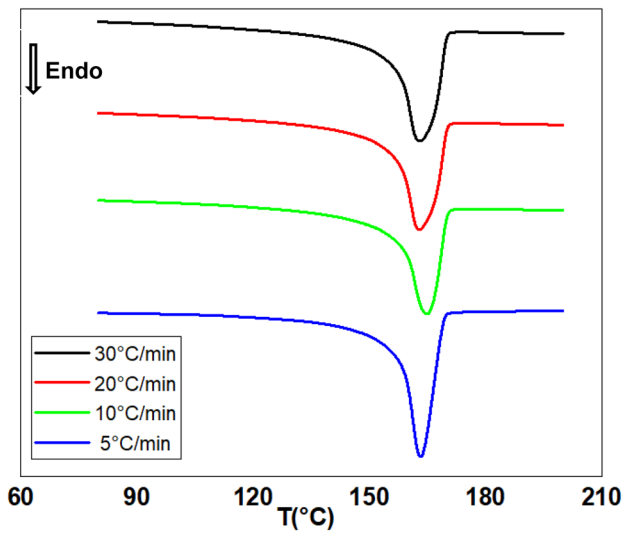

Fig. 12 Melting curves of iPP

Table 4 Crystallization fraction of iPP for different cooling rates

Cooling rate (°C min^{-1})	X_c(%)
5	55.7
10	52.5
20	44.2
30	38.7

solidification is an exothermic process, and the heat can develop thermal gradients in the sample during the phase. As a result, the thicker the sample, the more critical this problem is. Notably, the influence of the thickness of the sample and the cooling rate on the occurrence of thermal gradients during non-isothermal crystallization is still a missing spot.

Monasse and Haudin [48] estimated that for polypropylene samples, with 200-300 µm thickness, the variation in the thermal gradient between the sample and the hot stage was negligible. Moreover, Di Lorenzo and Silvestre [17] used films with 200 µm thickness and confirmed the existence of a thermal gradient in the samples. In our work, studied samples were about 80 µm and 150 µm. A cooling rate of 1 °C min^{-1} was used to cover a large range of experimental data.

Figure 7 represents the evolution of the spherulites radius with temperature for variously spaced spherulites in the same film with 150 µm thickness. The obtained plots show a significant difference between the evolution of the different spherulite radii. This variation is caused by the gradient between the platinum hot stage and the sample during solidification. To minimize the thermal gradient, thinner films are used with 100 µm of thickness.

The diameter of the iPP spherulite can be up to 40-90 µm, so the crystals find their free 3D space to grow radially. In this situation, insignificant gradients are expected in the same sample and between the furnace and the sample even during solidification, because the heat released during crystallization is very low due to the small mass of the used film. Therefore, it can be safely assumed that the effective temperature of the sample corresponds to that recorded by the hot stage. Generally, spherulite growth rates, G, are measured under isothermal conditions, where the growing spherulite radius R depends on the crystallization time t. In this study, G is estimated by the following equation for a constant cooling rate:

$$G = \frac{dR}{dt} = \frac{dR}{dT}\frac{dT}{dt}. \quad (8)$$

The time–temperature-diameter evolution diagram of the spherulite in a sample with 100-µm thickness is presented in Fig. 8. This diagram can be useful to study the evolution between of the spherulite diameter as a function of time and temperature. This figure shows the growth of the spherulites radius of the iPP with a cooling rate of 1 °C min^{-1}. The range of the crystallization temperature found by optical microscopy is higher than the one defined by DSC data. Hence, the development of the spherulite radius versus temperature gives a plot that will be later fitted to a polynomial equation showing a correlation coefficient of $R^2 > 0.9988$. Actually, it is a third-order equation (R = 0.0466T3 – 56.305T2 + 22686 T—3E + 04). Applying Eq. 8, the growth rate is then calculated as illustrated in Fig. 9.

Morphology and melting behavior after non-isothermal crystallization

The cooling rate obviously affects the final morphology, the spherulite size and even the crystallization of the iPP despite

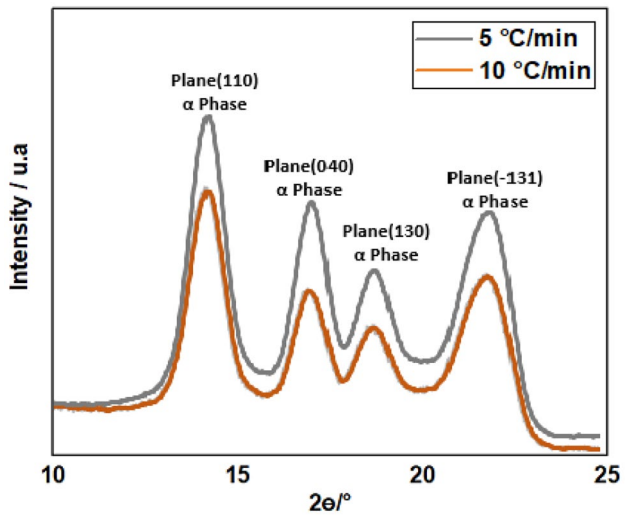

Fig. 13 WAXS intensity profiles of neat iPP for different cooling rates

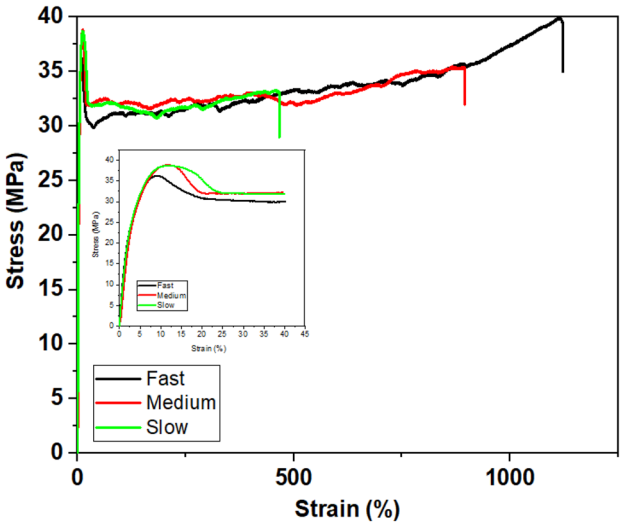

Fig. 14 Stress–strain curves of different films with various cooling rates

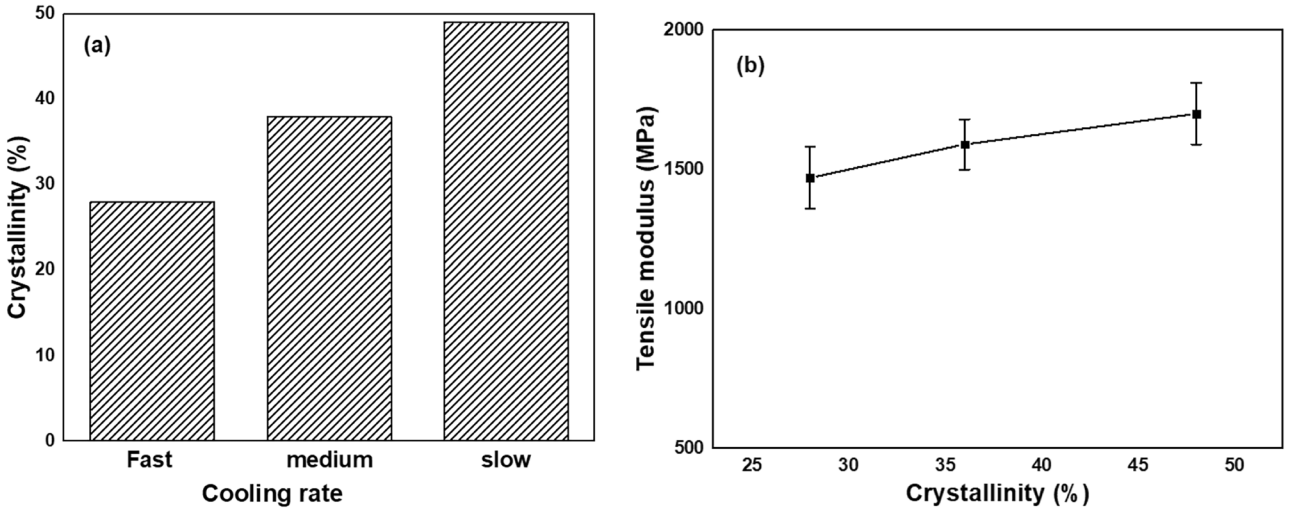

Fig. 15 Tensile modulus of iPP as a function of crystallinity degree at different cooling rates

its rapid crystallization. Thus, a neat iPP was subjected to heating after non-isothermal crystallization with different cooling rates to study the polymer morphology. The results of obtained endothermal peaks are presented in Figs. 10 and 11. According to these figures, it can be seen that the crystallization peak temperatures decrease with an increase in the cooling rates, and therefore the primary nucleation rises, which leads to a reduction in the spherulite size. Furthermore, the morphology depends also on the lamellar thickness.

According to the accompanying graphs in Fig. 12 and the data collected in Table 4, only the presence of the monoclinic crystalline structure α-phase can be affirmed. It is the most thermodynamically stable rather than the other three crystalline phases of the iPP, namely β, γ and smectic phases. The WAXS intensity profiles for different cooling rates are depicted in Fig. 13 while confirming the presence of the α-phase. In addition, the obtained profiles reveal the absence of a preferred orientation of the chains for different cooling rates (16, 49). Table 4 gives the global crystallinity rate (%) using the following equation:

$$X_c = \frac{\Delta H_{f_{\exp}}}{\Delta H_f{}^0} \tag{9}$$

where $\Delta H_{f_{\exp}}$ is the experimental crystallization enthalpy, and $\Delta H_f{}^0$ is the bulk enthalpy of polypropylene whose value is 177 J g^{-1}.

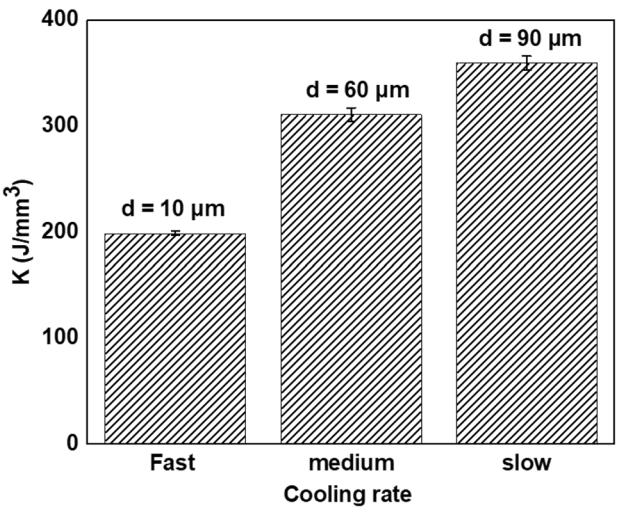

Fig. 16 Resilience (K) for different semi-crystalline states of iPP depending on the cooling rate

Mechanical properties after non-isothermal crystallization

At macroscopic scale

Tests were performed to evaluate the effect of the cooling rate and crystallinity on the mechanical properties of iPP polymer films. Specimens were fabricated at three different cooling rates in the hot stage under the same pressure: 60 °C min^{-1} (fast), 10 °C min^{-1} (medium), and 1 °C min^{-1} (slow). To have a uniform thickness for the different samples, a wedge was placed between two lamellar sheets. The crystallinity of each plate was determined using DSC.

The tensile properties were measured with 1BB specimens. Data were taken at a crosshead speed of 10 mm min^{-1}. In order to identify structure–property relations, the mechanical properties of thin films showing the structural state under different cooling rates were investigated. Uniaxial

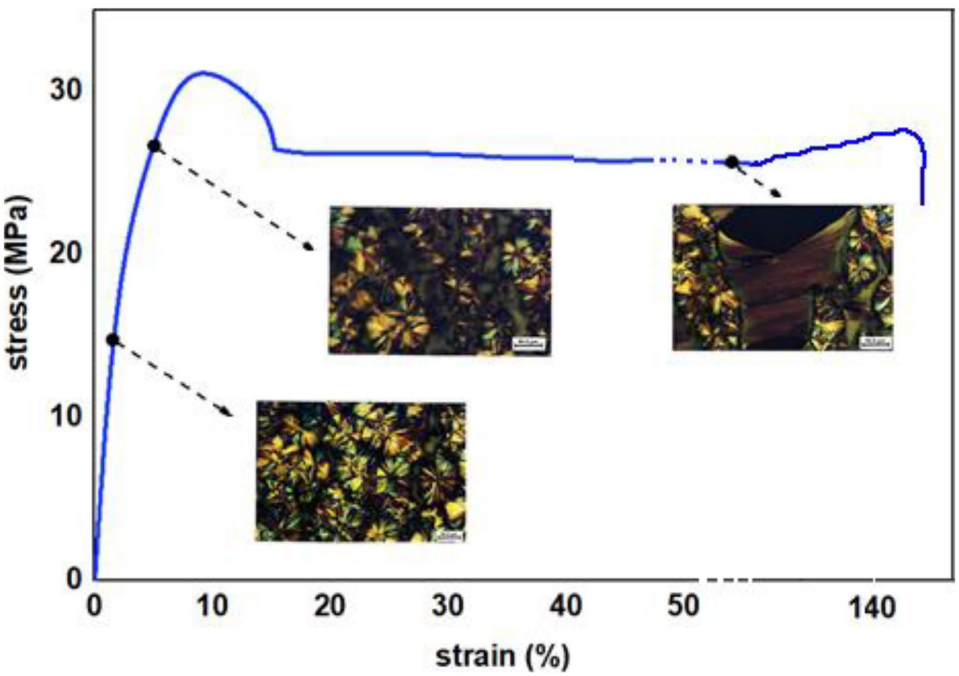

Fig. 17 Aggregate scale MOP under micromechanical tensile test

tensile tests were performed on 100 µm thick films prepared with linkam THM600. Young's modulus E and resilience K calculated from the stress–strain curves of these films will be discussed. The engineering stress–strain curves of different samples under a monotonic tensile test are presented in Fig. 14.

Figure 15a presents Young's modulus of the iPP as a function of the crystallinity degree at different cooling rates. Each point in Fig. 15b is the average of five data. As it can be seen, the tensile properties do not significantly vary over the range of evaluated crystallinity. Despite the insignificant variation in mechanical properties, the low cooling rates show good stability in the plastic part.

A pronounced augmentation in the resilience K (Fig. 16). Thus, the changes in K reveal that this property is very sensitive to structural differences depending on the cooling rate. It is worth noting that K(ϕ) depends on the ductile behavior with a significantly higher strain in the elastic phase for the slow cooling rate, while a rather brittle behavior is observed for the fast cooling rate.

It can be suggested that the mechanical quantities determined at small stresses and at small deformations such as Young's modulus E and resilience K are influenced differently by the microstructure of the semi-crystalline polymer. This difference underlines the variety and the complexity of factors affecting the mechanical properties of the semi-crystalline polymer. The dependence of the cooling rate on the crystallinity degree measured by DSC leads to a correlation between the observed values of E and the crystallinity degree. It can also be noted that even a significant difference in crystallization kinetics, spherulite size, microstructure and degree of crystallinity between thin films obtained using different cooling rates does not definitely represent the only parameters determining the tensile modulus of the polymer. Expectedly, other features like the crystal orientation, the heterogeneity in the microstructure and the pressure during manufacturing highly affect the strength of the semi-crystalline iPP at the elastic phase with small deformations.

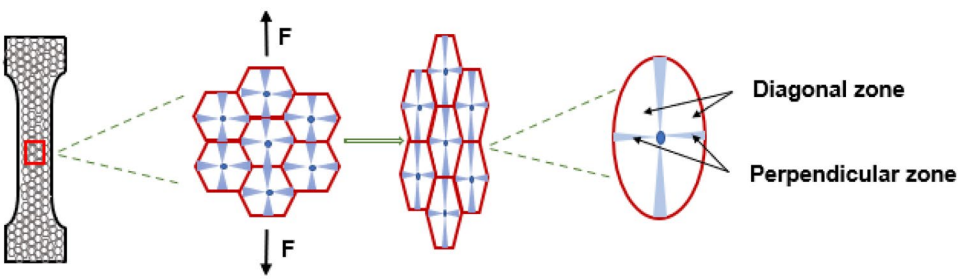

Fig. 18 Schematic of chronology of microstructure change

Another type of correlation is noticed. Basically, the resilience and the strain at rupture are influenced by the degree of crystallinity and the crystalline structure. It can be denoted that the improvement of resilience corresponds to the fine structures combined with bigger spherulites. However, rapid cooling and small spherulites demonstrate a homogenous plastic deformation at the macroscopic scale and an improvement of the strain at break.

In-situ tensile behavior: evolution of spherulites

Figure 17 shows the evolution of spherulites during micro tensile tests. Up to an elongation of 3%, the deformation seems to be homogeneous in the linear part, which corresponds to the elastic zone.

After that, local deformation appears at the scale of the spherulites which propagate in perpendicular and diagonal directions.

The schematic of this phenomenon is presented in Fig. 18, which shows the ellipsoidal form of the spherulites during or after loading. After striction, microcracks appear and spread in the same stress direction. This part also highlights the fibrillary structure at the level of the spherulites.

Actually, the growth of the strain at rupture may be related to the strength of the spherulite which itself can depend on an intra/inter rupture on the spherulite, and it is in progress to be investigated in our future work by studying different morphologies related to various process conditions.

Conclusion

The non-isothermal crystallization of the iPP was analyzed in this study using calorimetric data, which permitted the prediction of crystallization parameters by employing theoretical methods via Avrami and Ozawa's models. The obtained parameters of Avrami's model estimated the variation in the crystallization rate with the crystallization temperature at different cooling rates. In addition, the isoconversional analysis gave information about the activation energy and allowed the estimation of the temperature corresponding to the maximal crystallization rate. Microscopic observation confirmed that the crystallization peak temperatures decreased with an increase in cooling rates, and consequently primary nucleation rose, leading to a reduction in the spherulite size. Furthermore, the morphology depended also on the lamellar thickness. Moreover, the multi-scale mechanical results showed that the mechanical quantities determined at small amplitudes and at small deformations, like the E moduli, the resilience and the strain at rupture, were influenced differently by the microstructure of the semi-crystalline polymer, which could be related to an inter/intra spherulitic rupture.

Declarations

Conflict of interest There is no conflict and interest for this paper. All of persons had same contribution on this paper.

References

1. Nassiri H, Arabi H, Hakim S, Bolandi S (2011) Polymerization of propylene with Ziegler-Natta catalyst: optimization of operating conditions by response surface methodology (RSM). Polym Bull 67(7):1393–1411
2. Kunimitsu T, Toyoda K, Ikaga T, Kim K, Ohkoshi Y, Koike K (2020) High strength fiber obtained from a high stereoregularity metallocene catalyst-synthesized polypropylene. Polymer 202:122–654
3. Ding Q, Zhang Z, Dai X, Li M, Mai K (2014) Crystalline morphology and mechanical properties of isotactic polypropylene composites filled by wollastonite with β-nucleating surface. Polym Compos 35(8):1445–1452
4. Shyr T-W, Ko H-C, Wu T-M, Wu T-M (2019) Crystallisation and spherulite morphology of polylactide stereocomplex. Polym Int 68(1):141–150
5. Gallegos-Medrano KK, Escobar-Barrios V, Santamaría-Razo DA, Gutierrez-Castañeda EJ, Montesinos JV, Peña-Juarez MG et al (2021) Influence of chain length, particle size, and thermal treatment of dicarboxylic acid-functionalized titanium dioxide filler in polypropylene. J Mater Res 36(8):1718–1729
6. Lotz B, Wittmann JC, Lovinger AJ (1996) Structure and morphology of poly(propylenes): a molecular analysis. Polymer 37(22):4979–4992
7. Brückner S, Meille SV, Petraccone V, Pirozzi B (1991) Polymorphism in isotactic polypropylene. Prog Polym Sci 16(2):361–404
8. Stern C, Frick A, Weickert G (2007) Relationship between the structure and mechanical properties of polypropylene: Effects of the molecular weight and shear-induced structure. J Appl Polym Sci 103(1):519–533
9. Carotenuto C, Grassia L, Paduano LP, Minale M (2019 Non-Isothermal Crystallization Kinetics of an Ethylene-Vinyl-Acetate. II. Time-Temperature-Crystallinity-Superposition. Polym Eng Sci 59(12):2550–2556
10. Gradys A, Sajkiewicz P, Minakov AA, Adamovsky S, Schick C, Hashimoto T et al (2005) Crystallization of polypropylene at various cooling rates. Mater Sci Eng A 413–414:442–446
11. Wellen RMR, Canedo EL, Rabello MS (2015) Melting and crystallization of poly(3-hydroxybutyrate)/carbon black compounds. Effect of heating and cooling cycles on phase transition. J Mater Res 30(21):3211–3226
12. Keridou I, del Valle LJ, Funk L, Turon P, Franco L, Puiggalí J (2019) Non-Isothermal Crystallization Kinetics of Poly(4-Hydroxybutyrate) Biopolym Mole 24(15)
13. Wellen RMR, Canedo E, Rabello MS (2011) Nonisothermal cold crystallization of poly(ethylene terephthalate). J Mater Res 26(9):1107–1115
14. He M, Wei T, Zhang L, Jia Q (2016) Isothermal and nonisothermal crystallization kinetics of fully bio-based polyamides. Polym Eng Sci 56(7):829–836
15. Mubarak Y, Harkin-Jones EMA, Martin PJ, Ahmad M (2001) Modeling of non-isothermal crystallization kinetics of isotactic polypropylene. Polymer 42(7):3171–3182
16. Layachi A, Makhlouf A, Frihi D, Satha H, Belaadi A, Seguela R (2019) Non-isothermal crystallization kinetics and nucleation

behavior of isotactic polypropylene composites with micro-talc. J Therm Anal Calorim 138(2):1081–1095
17. Di Lorenzo ML, Silvestre C (1999) Non-isothermal crystallization of polymers. Prog Polym Sci 24(6):917–950
18. Wang G, Hou S, Cao J, Ding P, Shen J, Chen J (2018) Reinforcing and toughening isotactic polypropylene through shear-induced crystallization and β-nucleating agent induced crystallization. J Polym Res 25(11):233
19. Huan Q, Zhu S, Ma Y, Zhang J, Zhang S, Feng X et al (2013) Markedly improving mechanical properties for isotactic polypropylene with large-size spherulites by pressure-induced flow processing. Polymer 54(3):1177–1183
20. Pavlov VI (1971) Investigation of the effect of spherulite size on the strength and deformation characteristics of isotactic polypropylene films. Mater Sci 4(5):438–440
21. Nitta K, Odaka K (2009) Influence of structural organization on tensile properties in mesomorphic isotactic polypropylene. Polymer 50(16):4080–4088
22. Doyle MJ (2000) On the effect of crystallinity on the elastic properties of semicrystalline polyethylene. Polym Eng Sci 40(2):330–335
23. Fatahi S, Ajji A, Lafleur PG (2007) Correlation between different microstructural parameters and tensile modulus of various polyethylene blown films. Polym Eng Sci 47(9):1430–1440
24. Yasin S, Sun D, Memon H, Zhu F, Jian H, Bin Y et al (2018) Optimization of Mechanical and Thermal Properties of iPP and LMPP Blend Fibres by Surface Response Methodology. Polymers 10(10):1135
25. Mahmood N, Kolesov I, Glüge R, Altenbach H, Androsch R, Beiner M (2020) Influence of structure gradients in injection moldings of isotactic polypropylene on their mechanical properties. Polymer 200:122556
26. Dietz W (2016) Effect of cooling on crystallization and microstructure of polypropylene. Polym Eng Sci 56(11):1291–1302
27. Ray SS (2013) Clay-Containing Polymer Nanocomposites: From Fundamentals to Real Applications. Newnes 412 p
28. Righetti MC (2017) Crystallization of Polymers Investigated by Temperature-Modulated DSC. Materials 10(4):442
29. Buzarovska A (2004) Crystallization of polymers (2nd edition) Volume 2: Kinetics and mechanisms. Edited by Leo Mandelkern. Cambridge University Press, Cambridge. ISBN 0 521 81682 3. pp 478. Polym Int 2005;54(10):1466–1467
30. Zhang C, Lan Q, Zhai T, Nie S, Luo J, Yan W (2018) Melt Crystallization Behavior and Crystalline Morphology of Polylactide/Poly(ε-caprolactone) Blends Compatibilized by Lactide-Caprolactone Copolymer. Polymers 10(11):1181
31. Clark EJ, Hoffman JD (1984) Regime III crystallization in polypropylene. Macromolecules 17(4):878–885
32. Avrami M (1939) Kinetics of Phase Change I General Theory. J Chem Phys 7(12):1103–1112
33. Avrami M (1940) Kinetics of Phase Change II. Transformation-Time Relations for Random Distribution of Nuclei. J Chem Phys 8(2):212–224
34. Lorenzo AT, Arnal ML, Albuerne J, Müller AJ (2007) DSC isothermal polymer crystallization kinetics measurements and the use of the Avrami equation to fit the data: Guidelines to avoid common problems. Polym Test 26(2):222–231
35. Jeziorny A (1978) Parameters characterizing the kinetics of the non-isothermal crystallization of poly(ethylene terephthalate) determined by d.s.c. Polymer 19(10):1142–1144
36. Tian J, Yu W, Zhou C (2007) Crystallization behaviors of linear and long chain branched polypropylene. J Appl Polym Sci 104(6):3592–3600
37. Zhu X, Li Y, Yan D, Fang Y (2001) Crystallization behavior of partially melting isotactic polypropylene. Polymer 42(22):9217–9222
38. Gupta S, Yuan X, Chung TCM, Cakmak M, Weiss RA (2014) Isothermal and non-isothermal crystallization kinetics of hydroxyl-functionalized polypropylene. Polymer 55(3):924–935
39. Cho K, Li F, Choi J (1999) Crystallization and melting behavior of polypropylene and maleated polypropylene blends. Polymer 40(7):1719–1729
40. Ozawa T (1971) Kinetics of non-isothermal crystallization. Polymer 12(3):150–158
41. Evans UR (1945) The laws of expanding circles and spheres in relation to the lateral growth of surface films and the grain-size of metals. Trans Faraday Soc 41:365–374
42. Vyazovkin S (2018) Nonisothermal crystallization of polymers: Getting more out of kinetic analysis of differential scanning calorimetry data. Polym Crystallization 1(2):e10003
43. Kissinger HE (1957) Reaction Kinetics in Differential Thermal Analysis. Anal Chem 29(11):1702–1706
44. Achilias DS, Papageorgiou GZ, Karayannidis GP (2005) Evaluation of the Isoconversional Approach to Estimating the Hoffman-Lauritzen Parameters from the Overall Rates of Non-Isothermal Crystallization of Polymers. Macromol Chem Phys 206(15):1511–1519
45. Vyazovkin S, Sbirrazzuoli N (2003) Isoconversional Analysis of Calorimetric Data on Nonisothermal Crystallization of a Polymer Melt. J Phys Chem B 107(3):882–888
46. Benhacine F, Yahiaoui F, Hadj-Hamou AS (2014) Thermal Stability and Kinetic Study of Isotactic Polypropylene/Algerian Bentonite Nanocomposites Prepared via Melt Blending. Grohens Y éditeur J Polym 2014:426–470
47. Xing Y, Wang Y, Huang J, Fei Z, Liu Q, Chen X et al (2020) Study on the Mechanism and Kinetics of Waste Polypropylene Cracking Oxidation over the Mn2O3/HY Catalyst by TG–MS and In Situ FTIR. Ind Eng Chem Res 59(38):16569–16578
48. Monasse B, Haudin JM (1986) Thermal dependence of nucleation and growth rate in polypropylene by non isothermal calorimetry. Colloid Polym Sci 264(2):117–122
49. Labour T, Gauthier C, Séguéla R, Vigier G, Bomal Y, Orange G (2001) Influence of the β crystalline phase on the mechanical properties of unfilled and CaCO3-filled polypropylene I. Structural and mechanical characterisation. Polymer 42(16):7127–7135